Journal of Pharmaceutical Analysis 14 (2024) 244–258

Contents lists available at ScienceDirect

Journal of Pharmaceutical Analysis

journal homepage: www.elsevier.com/locate/jpa

Original article

Tanshinone IIA ameliorates energy metabolism dysfunction of pulmonary fibrosis using ^{13}C metabolic flux analysis

Baixi Shan [a, b], Haoyan Zhou [a, b], Congying Guo [a, b], Xiaolu Liu [a, b], Mingyu Wu [a, b], Rao Zhai [a, b], Jun Chen [a, b, *]

[a] State Key Laboratory of Natural Medicines, China Pharmaceutical University, Nanjing, 210009, China
[b] Department of Pharmacognosy, School of Traditional Chinese Pharmacy, China Pharmaceutical University, Nanjing, 210009, China

ARTICLE INFO

Article history:
Received 26 May 2023
Received in revised form
6 September 2023
Accepted 18 September 2023
Available online 21 September 2023

Keywords:
Pulmonary fibrosis
Tanshinone IIA
^{13}C-metabolic flux analysis
Metabolic reprogramming

ABSTRACT

Evidence indicates that metabolic reprogramming characterized by the changes in cellular metabolic patterns contributes to the pathogenesis of pulmonary fibrosis (PF). It is considered as a promising therapeutic target anti-PF. The well-documented against PF properties of Tanshinone IIA (Tan IIA) have been primarily attributed to its antioxidant and anti-inflammatory potency. Emerging evidence suggests that Tan IIA may target energy metabolism pathways, including glycolysis and tricarboxylic acid (TCA) cycle. However, the detailed and advanced mechanisms underlying the anti-PF activities remain obscure. In this study, we applied [U-^{13}C]-glucose metabolic flux analysis (MFA) to examine metabolism flux disruption and modulation nodes of Tan IIA in PF. We identified that Tan IIA inhibited the glycolysis and TCA flux, thereby suppressing the production of transforming growth factor-β1 (TGF-β1)-dependent extracellular matrix and the differentiation and proliferation of myofibroblasts *in vitro*. We further revealed that Tan IIA inhibited the expression of key metabolic enzyme hexokinase 2 (HK2) by inhibiting phosphoinositide 3-kinase (PI3K)/protein kinase B (Akt)/mammalian target of rapamycin (mTOR)/hypoxia-inducible factor 1α (HIF-1α) pathway activities, which decreased the accumulation of abnormal metabolites. Notably, we demonstrated that Tan IIA inhibited ATP citrate lyase (ACLY) activity, which reduced the collagen synthesis pathway caused by cytosol citrate consumption. Further, these results were validated in a mouse model of bleomycin-induced PF. This study was novel in exploring the mechanism of the occurrence and development of Tan IIA in treating PF using ^{13}C-MFA technology. It provided a novel understanding of the mechanism of Tan IIA against PF from the perspective of metabolic reprogramming.

1. Introduction

Pulmonary fibrosis (PF), characterized by extracellular matrix (ECM) remodeling and fibroblast proliferation, is a chronic, progressive, and restrictive pulmonary disorder that affects 3 million people globally with a poor survival rate [1]. It can be caused by various factors such as autoimmune disorders, drug-induced injuries, and traumatic injuries [2,3]. These injuries include alpha-smooth muscle actin (α-SMA)-producing myofibroblasts embedded within a type I collagen rich ECM and overlaid by exceedingly anomalous epithelium showing evidence of numerous phenotypic states, including apoptosis, senescence, and hyperplasia [4]. Controlling the occurrence and development of PF is of great significance for treating chronic lung diseases. Currently, two anti-fibrotic therapeutic agents, nintedanib and pirfenidone, have been developed to slow the progression of this complex disease [5]. However, although these drugs reduce the loss of lung function in patients with PF, their side effects on the gastrointestinal tract cannot be ignored. Thus, better therapeutic targets need to be identified on an urgent basis.

Metabolic reprogramming is a hallmark of cancer and has been found to significantly impact on the immune response and inflammation by modulating the differentiation and function of innate and adaptive immune cells [6,7]. Increasing evidence indicates that metabolic reprogramming is essential in the occurrence and development of non-oncological conditions such as PF [4]. Some shared metabolic signatures exist between cancer and PF, indicating a considerable mechanistic overlap [8,9]. Previous studies found that glycolysis increased during transforming growth factor (TGF)-β1-induced differentiation of myofibroblasts *in vitro* [10], implicating alterations in the expression of glycolytic enzymes

Peer review under responsibility of Xi'an Jiaotong University.
* Corresponding author. Department of Pharmacognosy, State Key Laboratory of Natural Medicines, China Pharmaceutical University, Nanjing, 210009, China.
E-mail address: chenj2002cpu@126.com (J. Chen).

https://doi.org/10.1016/j.jpha.2023.09.008

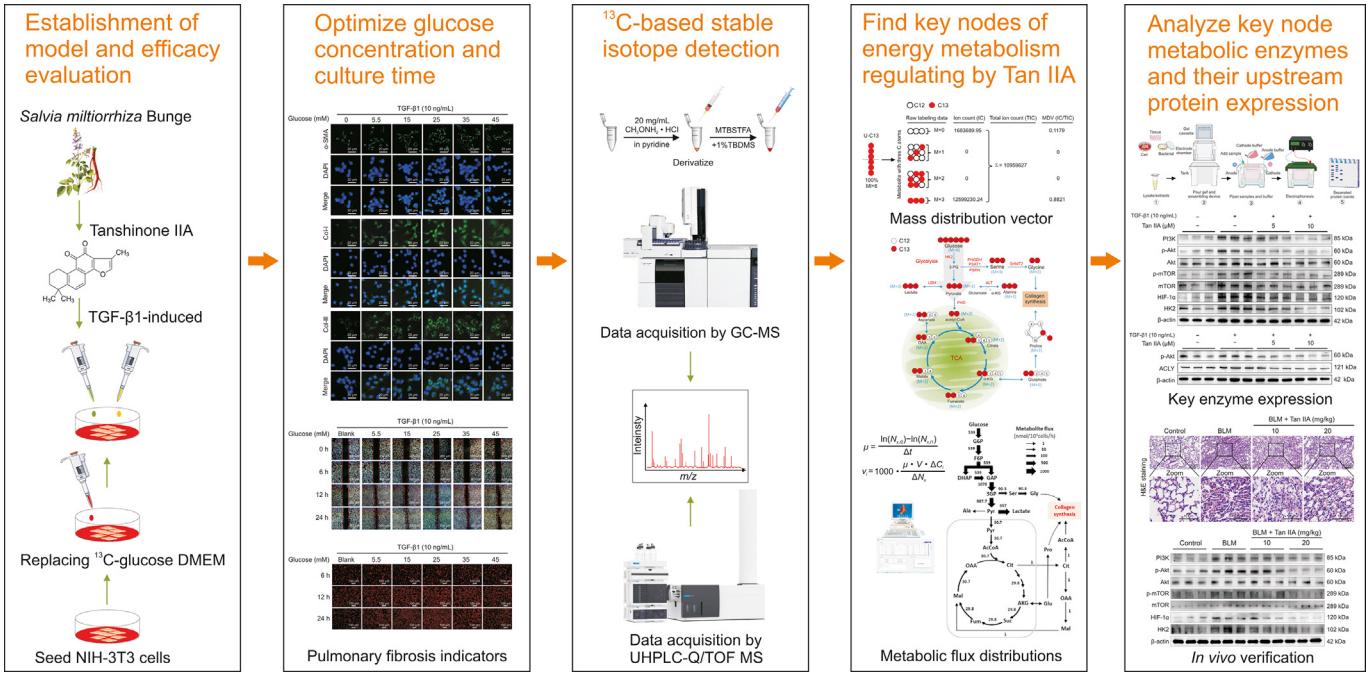

Fig. 1. The workflow of this study. GC-MS: gas chromatography-mass spectrometry; UHPLC-Q/TOF MS: ultra-high-performance liquid chromatography coupled with quadrupole time-of-flight mass spectrometry; Tan IIA: tanshinone IIA; TGF-β1: transforming growth factor-β1; DMEM: Dulbecco's modified Eagle medium.

(such as hexokinase 2 (HK2)), and glucose transporters in regulating key cellular signaling processes. Research has been suggested that it may be a consequence of the phosphoinositide 3-kinase (PI3K)/protein kinase B (Akt)/mammalian target of rapamycin (mTOR)/hypoxia-inducible factor 1α (HIF-1α) pathway downstream of transforming growth factor-β1 (TGF-β1) [11]. However, glucose utilization is highly variable and depends on genetics and the environment. Specific metabolic pathways, which are up-regulated due to metabolic reprogramming in fibrosis cells, are promising therapeutic targets in treating PF.

Chinese herbal medicines have been used to treat lung diseases for thousands of years. Several small molecular compounds derived from herbal medicines may serve as candidate drugs for PF treatment. Tanshinone IIA (Tan IIA), an essential lipophilic diterpene extracted from the root of a Chinese herb called *Salvia miltiorrhiza* Bunge, has been extensively studied due to its various pharmacological actions [12]. Previous studies have demonstrated that Tan IIA effectively attenuates fibrosis, such as renal, peritonea, and PF [13]. The anti-fibrosis properties of Tan IIA have been fully proved, which are mainly attributed to its potent antioxidant and anti-inflammatory efficacy [14]. However, the mechanisms by which Tan IIA regulates metabolic reprogramming in fibrosis are still poorly understood. It is crucial to comprehend how Tan IIA generates appropriate network responses that allow cells to function effectively under varying environmental conditions.

Many metabolites are involved in multiple metabolic pathways and although their overall measured concentrations may not change, they may show clear changes in a particular pathway [15]. Stable isotope tracer glucose metabolic flux analysis (MFA) introduces a tracer (^{13}C, ^{15}N, or ^{2}H) into a biological system. As a labeled substrate (e.g. [U-^{13}C] glucose) is metabolized by the cell, an enzymatic reaction rearranges the carbon atoms to produce a specific labeling pattern in the downstream metabolite, which can be detected by gas chromatography-mass spectrometry (GC-MS) or liquid chromatography-mass spectrometry (LC-MS) to obtain isotopic ratios of these metabolites [16,17]. By combining measurements of cellular growth rates with quantification of glucose uptake and lactate secretion rates, a quantitative map of cellular metabolism is generated by assigning flux values and confidence intervals for each estimated flux to the reactions in the network model. This approach provides a more in-depth and accurate description of the metabolic process [18,19].

In this study, we found that Tan IIA decreased the metabolism of myofibroblast cells in glycolysis and tricarboxylic acid (TCA) cycle and reduced the inflow of carbon source for metabolite generation in the metabolic network via ^{13}C-MFA (Fig. 1). We further demonstrated that Tan IIA had strong anti-PF effects in myofibroblast by inhibiting PI3K/Akt/mTOR/HIF-1α/HK2 pathway, leading to cell growth arrest and metabolic inhibition *in vitro*. More excitingly, we discovered a new anti-PF mechanism of Tan IIA by inhibiting cytosol citrate consumption and acetyl coenzyme production, which resulted in the obstruction of collagen synthesis. Finally, *in vivo* experiments in mouse models were used for further verification. Our findings provided novel insights into the biological actions of Tan IIA under PF conditions and a better understanding of the molecular events responsible for energy metabolism. This detailed understanding helped elucidate how Tan IIA participated in metabolic reprogramming.

2. Materials and methods

2.1. Reagents and chemicals

Tan IIA (purity > 98%), [U-^{13}C]-glucose, L-serine, L-glycine, L-lactic acid, L-alanine, pyruvate, L-malic acid, succinate, fumarate, L-glutamic acid, citric acid, α-ketoglutaric acid, L-asparatic acid, and L-proline were purchased from Shanghai Yuanye Biotechnology Co., Ltd (Shanghai, China). Recombinant human TGF-β1, Yefluor 488 EdU imaging kit, and cell cycle and apoptosis analysis kit were purchased from Yeasen (Shanghai, China). Sulforaphane (SFN), dimethyl sulfoxide (DMSO) and methoxyamine hydrochloride

were purchased from Sigma-Aldrich (St. Louis, MO, USA). D-glucose was purchased from Aladdin (Shanghai, China). Dulbecco's modified Eagle medium (DMEM), minimum essential medium (MEM), and 0.25% trypsin were purchased from Gibco (Carlsbad, CA, USA). Cell counting kit-8 (CCK-8) was purchased from Vazyme (Nanjing, China). SB 204990 was purchased from MedChemExpress (Princeton, NJ, USA). BTA was purchased from Macklin (Shanghai, China). Glucose assay kit was purchased from Elabscience (Wuhan, China). Lactate assay kit was purchased from Nanjing Jiancheng Bioengineering Institute (Nanjing, China). *N-tert*-butyldimethylsilyl-*N*-methyltrifluoroacetamide was purchased from Acmec (Shanghai, China). Triton ×100, hoechst33342, antifade mounting medium and 4',6-diamidino-2-phenylindole (DAPI) were purchased from Beyotime (Shanghai, China).

2.2. Cell culture

NIH-3T3 and MRC-5 cells were purchased from Cell Bank, Chinese Academy of Science (Shanghai, China). NIH-3T3 cells were cultured in DMEM with 10% fetal bovine serum (FBS) and 1% penicillin/streptomycin in a humidified incubator with 5% CO_2 at 37 °C. MRC-5 cells were cultured in MEM with 10% FBS and 1% penicillin/streptomycin in a humidified incubator with 5% CO_2 at 37 °C. For serum starvation of cells, after the medium was removed, cells were washed with phosphate buffered solution (PBS) for twice and added to the medium without FBS before proceeding with further experiments.

2.3. Cell viability

Cell viability was measured with CCK-8. Procedure was carried out according to the manufacturer's instructions.

2.4. Quantification of glucose consumption and lactate production

NIH-3T3 cells were induced by TGF-β1 (10 ng/mL) and treated with Tan IIA (10 μM) for 24 h. Medium was taken at 0 h and 24 h for glucose and lactate detection by the glucose assay kit (E-BC-K234-M, Elabscience) and lactate assay kit (A019-2-1, Nanjing Jiancheng Bioengineering Institute) according to the manufacturer's protocol.

2.5. Determination of external rates

The external rate measurement method is based on the previously published articles [18]. To quantify intracellular metabolic fluxes, we first need to quantify external rates. This includes measuring glucose uptake and lactate secretion. Of note, the growth rate of the cells must be determined. The following formula is applicable to the calculation of the growth rate of continuously dividing cells:

$$\mu = \frac{\ln(N_{t2}) - \ln(N_{t1})}{\triangle t}$$

Here N is the number of cells (typically expressed in millions of cells), and μ (1/h) is the growth rate.

For exponentially growing cells, external rates (r, in units nmol/10^6 cells/h) can be calculated as follows:

$$r = 1000 \cdot \frac{\mu \cdot V \cdot \triangle c}{\triangle N}$$

Here Δc (mmol/L) is the change in concentration of metabolite, ΔN is the change in cell number (expressed in millions of cells), V (mL) is the culture volume, and μ (1/h) is the growth rate.

2.6. Metabolic flux experiments using [U-^{13}C] glucose and analysis by GC-MS

2.6.1. Labeled ^{13}C-glucose assay

NIH-3T3 cells were grown in culture dish at a density of 1×10^6 cells. Following attachment on the bottom of dish, the original medium is discarded, and the PBS buffer is gently washed twice. Culture medium was replaced by 25 mM of [U-^{13}C] glucose medium supplemented without FBS. Then, the cells were divided into five groups: control, TGF-β1 (10 ng/mL), TGF-β1 + Tan IIA (5 μM), TGF-β1 + Tan IIA (10 μM) and TGF-β1 + SB204990 (15 μM) and cultured in incubator for 24 h ($n = 3$).

2.6.2. Extraction of metabolites

The extraction method has been described in previous studies [20]. Briefly, the cells were washed twice with pre-cold PBS, then quickly added 2 mL of pre-cooled 80% methanol (−80 °C) to quench cell metabolism, and collected by scraping the culture plate. The entire extraction process was performed on ice. The harvested cells were placed in a new Eppendorf tube (EP), whirled for 3 min, lysed by ultrasound for 2 min, and left in a refrigerator at −80 °C for 30 min. After centrifugation at 12,000 *g* for 10 min at 4 °C, the supernatant was transferred and dried completely with nitrogen gas.

2.6.3. Derivatization of metabolites

The dried residue was rehydrated by adding 30 μL of 20 mg/mL methoxyamine hydrochloride in pyridine, and heated at 37 °C for 1.5 h. After a quick centrifugation, 30 μL of N-(t-butyldimethylsilyl)-N-methyltrifluoroacetamide (MTBSTFA) + 1% *tert*-butyldimethylsilyl (TBDMS) was added into the mixture and derivatized at 55 °C for 60 min [21]. The derivatized samples were centrifuged for 5 min at 12,000 *g*, and the supernatants were transferred to a GC vial for GC-MS analysis.

2.6.4. GC-MS analysis

A modified GC-MS method was employed [22]. Instrumental analysis was performed on an Agilent 8,890 GC system equipped with a HP-5MS capillary column (30 m × 250 μm × 0.25 μm-phase thickness; Agilent J&W Scientific, Santa Clara, CA, USA), connected to an Agilent 7,000D Mass Spectrometer operating under ionization by electron impact (EI) at 70 eV. After optimizing the inlet temperature, split ratio, helium flow rate and heating rate, samples were injected in a split ratio of 1/10, with an injection volume of 1 μL. The GC oven temperature was initially set to 80 °C for 2 min before being increased to 280 °C at a rate of 7 °C/min. The temperature was held at 280 °C for a total run time of 35.5 min. The experiment involved maintained a helium flow rate of 1 mL/min. The ion source, MS quad temperature, interface, and inlet temperature were set to 230 °C, 150 °C, 280 °C, and 250 °C, respectively. Mass spectra were recorded in the m/z range of 50—700 while in mass scan mode.

2.6.5. ^{13}C-based stable isotope analysis

The GC-MS data were analyzed to determine the isotope labeling and quantities of metabolites. In this context, M_0 (without any heavy isotopes) to M_n (up to M_6) refers to the isotopes that contain n heavy atoms in the molecule. Details of the metabolites tested are listed in Tables S1 and S2. To determine the ^{13}C labels, the mass distributions of known metabolite fragments were extracted from the corresponding chromatographic peaks. These mass distributions are then normalized by dividing them by the sum of M_0 to M_6. In this study, we corrected the labeling of all measured metabolites in cells that were treated with ^{13}C-labeled medium. We did this by using the natural isotope distribution that we assayed from cell samples that were treated with unlabeled carbon sources, as described in previous reports [22], ensuring that a stable state of

cellular isotopes is a prerequisite for successful experiments using the MFA method. We extracted m+2 and m+3 isotopic metabolites from [U-^{13}C]-glucose cultured NIH-3T3 cells at 12 h and 24 h according to the cell growth state, and mass isotope distributions (MID) were calculated. The time to reach isotopic steady state was determined based on the change in metabolite ^{13}C labelling ratios over time. After 24 h of cell culture, the ^{13}C-labeled ratios of glycolysis and TCA first cycle metabolites were stable, indicating that the cells reached and maintained isotopic steady state at 24 h.

2.7. Ultra-high-performance liquid chromatography coupled with quadrupole time-of-flight mass spectrometry (UHPLC-QTOF-MS) metabolic flux analysis

The medium was abandoned and washed twice times with PBS. Cells were extracted by adding 2 mL of 80% methanol pre-cooled at −80 °C, ultrasound and vortexed for 1 min, then left at −80 °C for 30 min, ultrasound and vortexed again for 1 min, and centrifuged at 12,000 *g* for 10 min at 4 °C. Supernatants were transferred to a new centrifuge tube, dried under nitrogen flow, and stored at −80 °C. The dried sample was resuspended in 60 μL 50% acetonitrile, incubated on ice for 30 min and 4 °C centrifuged at 12,000 *g*, 5 min. The 50 μL supernatant was transferred to a feeder vial containing an inset tube and injected for analysis.

Ultra-performance liquid chromatography-tandem mass spectrometry (UPLC-MS/MS) analysis was performed on an Agilent UPLC system connected to a QTOF 6546 MS (Agilent). Samples were separated on a Waters BEH Amide column (100 mm × 2.1 mm, 1.7 μm; Wexford, Ireland) using a linear gradient elution system with mobile phases of (A) 20 mM ammonium acetate and 20 mM ammonium hydroxide in 95% water (water:acetonitrile (95:5, *V/V*)), pH 9 and (B) acetonitrile solution. The gradient elution conditions were as follows: 0–3 min, 95% B; 3–5 min, 86% B; 5–6 min, 76% B; 6–12 min, 76% B; 12–15 min, 60% B; 15–17 min, 6% B. The column temperature was 30 °C. The injection volume was 4 μL. The flow rate was 400 μL/min. Chromatographic column separated analytes were ionized in positive (ESI+) and negative (ESI−) mode in an electrospray ionization source. The positive (ESI+) mass spectrometry parameters were: gas temperature, 320 °C; gas flow rate, 9 L/min; nebulizer, 35 psi; sheath gas temperature, 350 °C; sheath gas flow rate, 11 L/min; nozzle voltage, 1,000 V; VCap, 4,000 V; fragmenter, 80 V; and octopoleRFPeak, 750 V. The negative (ESI−) mass spectrometry parameters were: consistent with (ESI+), except that nozzle voltage, 500 V; VCap, 3,500 V. Data analysis were carried out in MassHunter Quant software. For a comprehensive list of metabolites, retention times, etc., please refer to Table S3.

2.8. 5-ethynyl-20-deoxyuridine (EdU) assay

Cell proliferation rates were determined by the uptake of EdU into DNA using Yefluor 488 EdU imaging kits according to the manufacturer's instructions. In short, the cells were seeded in a 96-well plate and cultured for 12 or 24 h. Then, we added 10 μM of EdU working solution to the plates and incubated them for 2 h at 37 °C. After incubation, we treated the cells with a 4% polyformaldehyde solution at room temperature for 15 min. The cells were first washed with PBS and then permeabilized with 0.5% Triton X-100 at room temperature for 20 min. Following another wash with PBS, the cells were incubated with the click-iT reaction mixture in darkness for 30 min. Finally, the cells were stained with hoechst staining solution and fluorescence was detected by Olympus IX53 microscope (Olympus, Tokyo, Japan) after washing.

2.9. Flow cytometry analysis

To analyze the cell cycle, NIH-3T3 cells were treated with Tan IIA (5 μM and 10 μM) for 24 h. We then digested the adhesion cells with 0.25% trypsin and fixed a total of 1×10^6 cells with 70% ethanol overnight at 4 °C. Next, we processed the cells using the cell cycle and apoptosis analysis kit in accordance with the manufacturer's instructions. Finally, the flow cytometry data were generated on BD FACSCelesta and analyzed with FlowJo v10 software.

2.10. Scratch assay

Cells were inoculated in uncoated 6-well plates at a density of 6×10^4 cells/well and cultured in DMEM containing 10% FBS for 12 h until reaching 80% confluency. Cell monolayers were manually scraped with a p200 pipette, then washed with PBS three times, and immediately replaced with serum-free fresh medium. After scratching, cells were observed under a phase contrast microscope (Olympus) at 6, 12, and 24 h, respectively, and digital photographs were taken by matching reference points. The percent cell migration was calculated using ImageJ software.

2.11. Western blotting

The western blotting procedure was carried out according to established protocols [23,24]. Briefly, the cells or tissue were washed twice with cold PBS and then lysed with radioimmune precipitation assay (RIPA) buffer containing 1 mM protease and phosphatase inhibitor. The protein extracts were separated by sodium dodecyl sulfate polyacrylamide gel electrophoresis (SDS-PAGE) and transferred to nitrocellulose membranes. The membranes were blocked with 5% (*m/V*) skim milk and incubated with the following primary antibodies: rabbit anti-collagen type I (14695-1-AP, Proteintech, Chicago, IL, USA), rabbit anti-collagen type III (22734-1-AP, Proteintech), rabbit anti-α-smooth muscle actin (#19245, Cell Signaling Technology, Boston, MA, USA), rabbit anti-phospho-Akt (Ser473) (66444-1, Proteintech), rabbit anti-Akt (10176-2-AP, Proteintech), mouse anti-HIF-1α (66730-1-lg, Proteintech), rabbit anti-PI3K (WL02240, Wanleibio, Shenyang, China), rabbit anti-mTOR (WL02477, Wanleibio), rabbit anti-phosphor-mTOR (WL03694, Wanleibio), rabbit anti-hexokinase 2 (WL02454, Wanleibio), rabbit anti-ACLY (R23558, Zenbio, Chengdu, China), rabbit anti-β-actin (81115-1-RR, Proteintech), and rabbit anti-GAPDH (10494-1-AP, Proteintech). Following three times washes with TBST buffer, the membranes were incubated with secondary antibodies: goat anti-rabbit (AB0101, Abways, Shanghai, China), and goat anti-mouse (BS12478, Bioworld Technology, Nanjing, China). The blots were finally detected by enhanced chemiluminescence (ECL) kit (Yeasen).

2.12. Quantitative real-time polymerase chain reaction (PCR)

The RNA-easy™ isolation reagent from Vazyme was used to extract total RNA from NIH-3T3 cells following the manufacturer's protocol. Gene-specific primer pairs for glyceraldehyde 3-phosphate dehydrogenase (GAPDH), alpha-smooth muscle actin (α-SMA), collagen I (Col-I), and collagen III (Col-III) are provided in Table S4. PCR conditions are consistent with previous studies [23]. We expressed semiquantitative real-time PCR data for each target gene as $2^{-\triangle\triangle Ct}$ relative quantitation versus endogenous GAPDH, with error bars representing the standard error of the mean of triplicate reactions.

2.13. Immunofluorescence

NIH-3T3 cells were initially plated on glass coverslips in 24-well tissue culture plates. After 24 h, the cells were rinsed in phosphate-

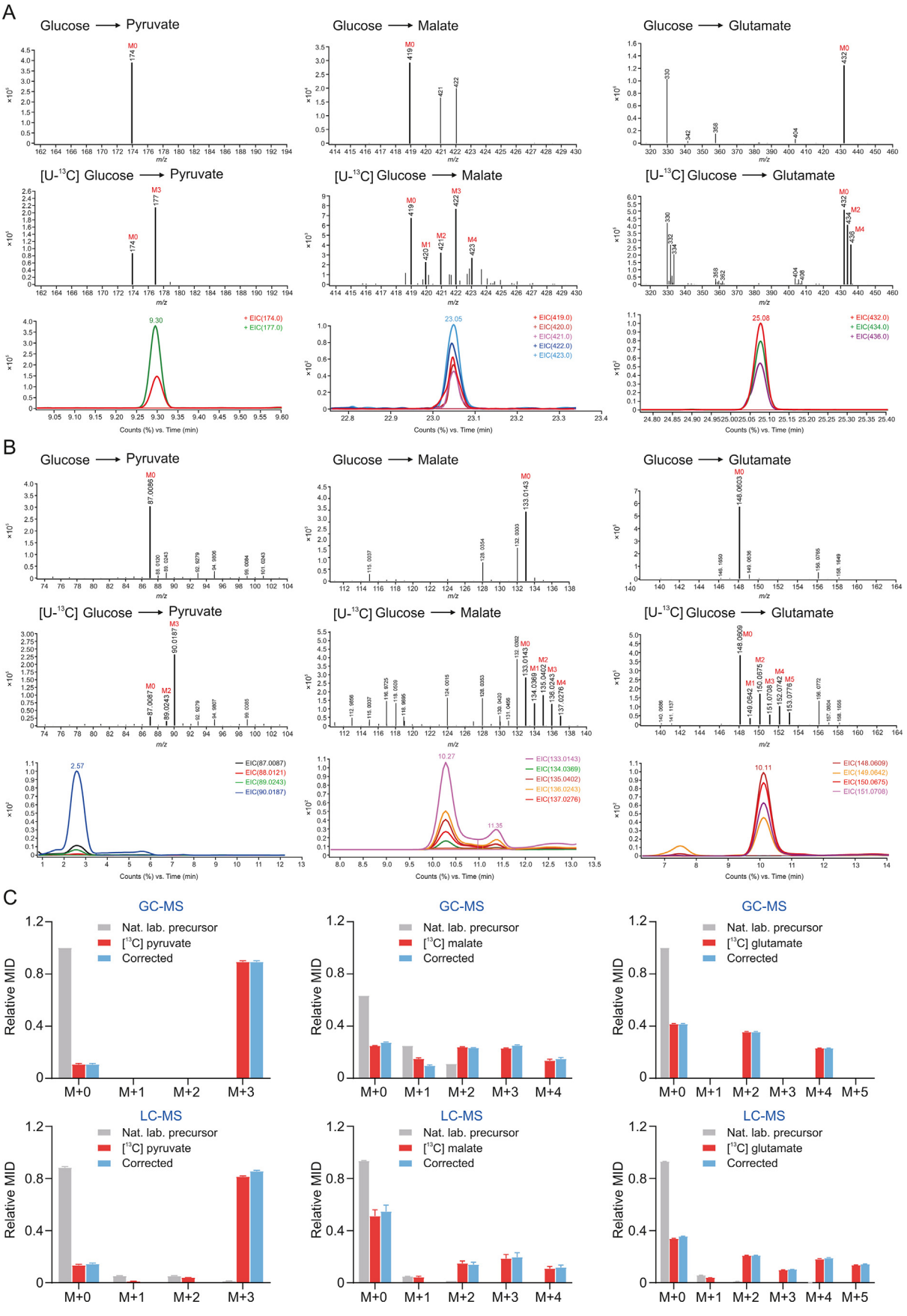
A
Glucose ⟶ Pyruvate
Glucose ⟶ Malate
Glucose ⟶ Glutamate
[U-13C] Glucose ⟶ Pyruvate
[U-13C] Glucose ⟶ Malate
[U-13C] Glucose ⟶ Glutamate
+ EIC(174.0)
+ EIC(177.0)
+ EIC(419.0)
+ EIC(420.0)
+ EIC(421.0)
+ EIC(422.0)
+ EIC(423.0)
+ EIC(432.0)
+ EIC(434.0)
+ EIC(436.0)
Counts (%) vs. Time (min)
B
Glucose ⟶ Pyruvate
Glucose ⟶ Malate
Glucose ⟶ Glutamate
[U-13C] Glucose ⟶ Pyruvate
[U-13C] Glucose ⟶ Malate
[U-13C] Glucose ⟶ Glutamate
EIC(87.0087)
EIC(88.0121)
EIC(89.0243)
EIC(90.0187)
EIC(133.0143)
EIC(134.0369)
EIC(135.0402)
EIC(136.0243)
EIC(137.0276)
EIC(148.0609)
EIC(149.0642)
EIC(150.0675)
EIC(151.0708)
Counts (%) vs. Time (min)
C
GC-MS
LC-MS
Nat. lab. precursor
[13C] pyruvate
[13C] malate
[13C] glutamate
Corrected
Relative MID
M+0
M+1
M+2
M+3
M+4
M+5

buffered saline and fixed in 4% paraformaldehyde at room temperature. Subsequently, the cells were permeabilized with 0.3% Triton X-100, followed by two rinses with PBS. The coverslips were then blocked for 1 h in blocking buffer (0.3% BSA in PBS) and incubated with primary antibody (α-SMA, Col-I, or Col-III at a 1:200 dilution) in PBS overnight at 4 °C. After washing the samples twice with PBS, they were incubated with a fluorescent-labeled secondary antibody and DAPI staining was applied. The resulting fluorescence images were captured using a fluorescence microscope, Olympus IX53.

2.14. Animal experiments

Female C57BL/6 mice (20 ± 2 g) were purchased from Zhejiang Vital River Laboratory Animal Technology Co., Ltd (Jiaxing, China). All mice were maintained under standard conditions 12-h light/dark cycles with free access to food and water. All procedures were conducted in accordance with the guidelines of Chinese Experimental Animals Administration Legislation. The animal care and experimental procedures were approved by the Animal Ethics Committee of the China Pharmaceutical University (Approval number: 2022–05–041). The experiment of bleomycin (BLM)-induced PF in mice was performed as our previous method [14,25]. In brief, after BLM infusion, mice were administrated with Tan-IIA (10 and 20 mg/kg) or 0.5% CMC-Na solution as vehicle for 21 consecutive days. The mice were euthanized for collection of lung samples on day 21 after BLM treatment. Right lobes were quickly frozen in liquid nitrogen followed by storing at −80 °C for Western blot analysis. Left lobes were directly fixed in 4% paraformaldehyde for histological examination.

2.15. Hematoxylin-eosin (HE) staining

The lung left lobe tissues were fixed with 4% paraformaldehyde, dehydrated, and embedded in paraffin, and cut into 5-μm slices for subsequent experiments. Slices were stained with HE. Finally, the slices were mounted for observation under a microscope.

2.16. Statistical analysis

The data in this work were reported as means ± standard deviation (SD) or means ± standard error of the mean (SEM). Statistical analysis was performed using GraphPad Prism 8.0 (San Diego, CA, USA) by applying two-tailed Student's *t* tests (comparison between two groups) or one-way analysis of variance (ANOVA) (comparing among more than two groups), and $P < 0.05$ was considered statistically significant.

3. Results

3.1. Optimization of NIH-3T3 cell culture environment with glucose as a carbon source

First, we assessed the effects of glucose on cell viability, proliferation, and migration by culturing NIH-3T3 in a medium with different concentrations of glucose. As shown in Figs. S1A–C, we used a CCK-8 assay to assess the viability of NIH-3T3 cells treated with different doses of glucose for 6, 12, and 24 h. We found that 25 mM glucose exhibited high cell viability in all three culture time points, which was consistent with the results of cell growth (Fig. S1D). Next, we added TGF-β1 stimulating fibroblasts to differentiate into myofibroblasts and observed their growth and viability. We found that the cells cultured with 25 mM glucose also exhibited higher cell viability and cell density after adding TGF-β1 (Figs. S1E and S2A). Additionally, the EdU incorporation assay was used to detect the proliferation of myofibroblasts at different glucose concentrations. The results showed that myofibroblasts cultured with 25 mM glucose showed higher proliferation after 12 and 24 h of cultivation (Figs. S2B and C). In PF, myofibroblasts exhibit the characteristics of vigorous metabolism and abnormal proliferation similar to tumor cells. To examine the effect of increased glucose levels on myofibroblast migration *in vitro*, we conducted a scratch assay. As shown in Fig. S2D, myofibroblast migration was inhibited in cells cultured at higher glucose concentrations (35 and 45 mM). This inhibition was observed within 12 h. In contrast, the migration of cells incubated with 25 mM glucose was slightly faster than that at other concentrations in 24 h.

Studies revealed that TGF-β1-induced myofibroblast differentiation and collagen synthesis were inhibited in the absence of extracellular glucose [26]. We measured the expression of epithelial–mesenchymal transition-associated proteins and mRNA in NIH-3T3 cells cultured with different concentrations of glucose after 24 h of TGF-β1 induction to investigate the role of glucose in the epithelial-mesenchymal transition of TGF-β1-treated NIH-3T3 cells. Compared with the blank group (0 mM), the expression of α-SMA, Col-I and Col-III proteins, and mRNA increased in cells cultured in glucose, notably, the expression of α-SMA, Col-I and Col-III at the protein and mRNA levels decreased gradually in cells cultured with higher concentrations of glucose (Fig. S2E). Additionally, we further used immunofluorescence technology to analyze the epithelial-mesenchymal transition-related proteins to understand the protein expression more comprehensively, and the results were consistent with those of western blotting (Fig. S3).

Based on the aforementioned experimental results, we found that myofibroblasts displayed high cell viability, migration, and proliferation, and strong epithelial-mesenchymal transition-related protein expression in a 25 mM glucose medium. Therefore, 25 mM glucose was considered as the best concentration medium, and hence the subsequent experiments were conducted with the medium containing 25 mM glucose. Further, we explored the appropriate serum concentration in the medium at 25 mM glucose concentration to determine the effect of serum in the myofibroblast medium. Cultures in a medium containing 10% serum for 12 and 24 h showed relatively good cell survival (Figs. S4A–C). However, we found that the expression of epithelial-mesenchymal transition-related proteins (α-SMA, Col-I, and Col-III) gradually decreased with increasing serum concentration (Figs. S4D–F) and only showed a higher expression in the serum-free medium. We believed that the presence of serum interfered with the experimental results; therefore, all subsequent experiments were conducted in the serum-free medium.

3.2. Comparison of isotope labeled metabolite distribution in fibroblasts cultured with [U-^{13}C] glucose using GC-MS and LC-MS

After determining the optimal cell culture environment, we next established an analytical method for metabolic flux based on LC-MS and GC-MS platforms, and analyzed and compared the responses of both LC-MS and GC-MS to metabolites and their isotopic distributions. The ion chromatograms and mass spectra of

Fig. 2. Comparison of isotope labeled metabolite distribution in fibroblasts cultured with [U-^{13}C] glucose using gas chromatography-mass spectrometry (GC-MS) and liquid chromatography-mass spectrometry (LC-MS). (A) Detection of pyruvate, malate, and glutamate isotopomer distribution by GC-MS. (B) Detection of pyruvate, malate, and glutamate isotopomer distribution by LC-MS. (C) Mass isotopomer distribution and natural isotopomer correction of pyruvate, malate, and glutamate. MID: mass isotope distributions.

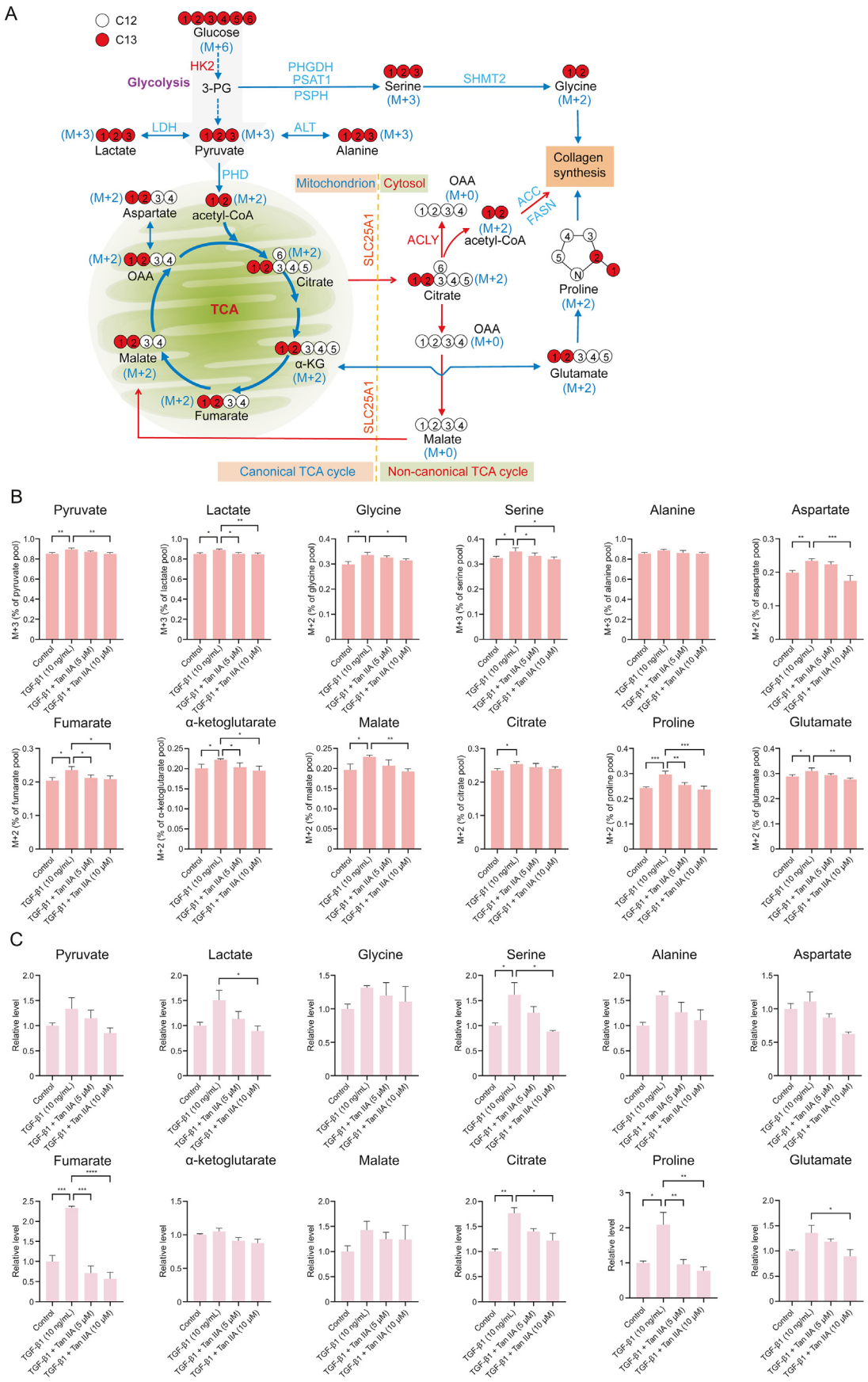

Fig. 3. Metabolite information of cell samples treated with labeled carbon sources [U-^{13}C] glucose. (A) Schema showing the [U-^{13}C] glucose metabolism. ^{13}C distribution of *de novo* serine-glycine synthesis, glycolysis and the first turn of the tricarboxylic acid (TCA) cycle with [U-^{13}C]-glucose (labeled at all six carbons). (B) NIH-3T3 cells induced by transforming

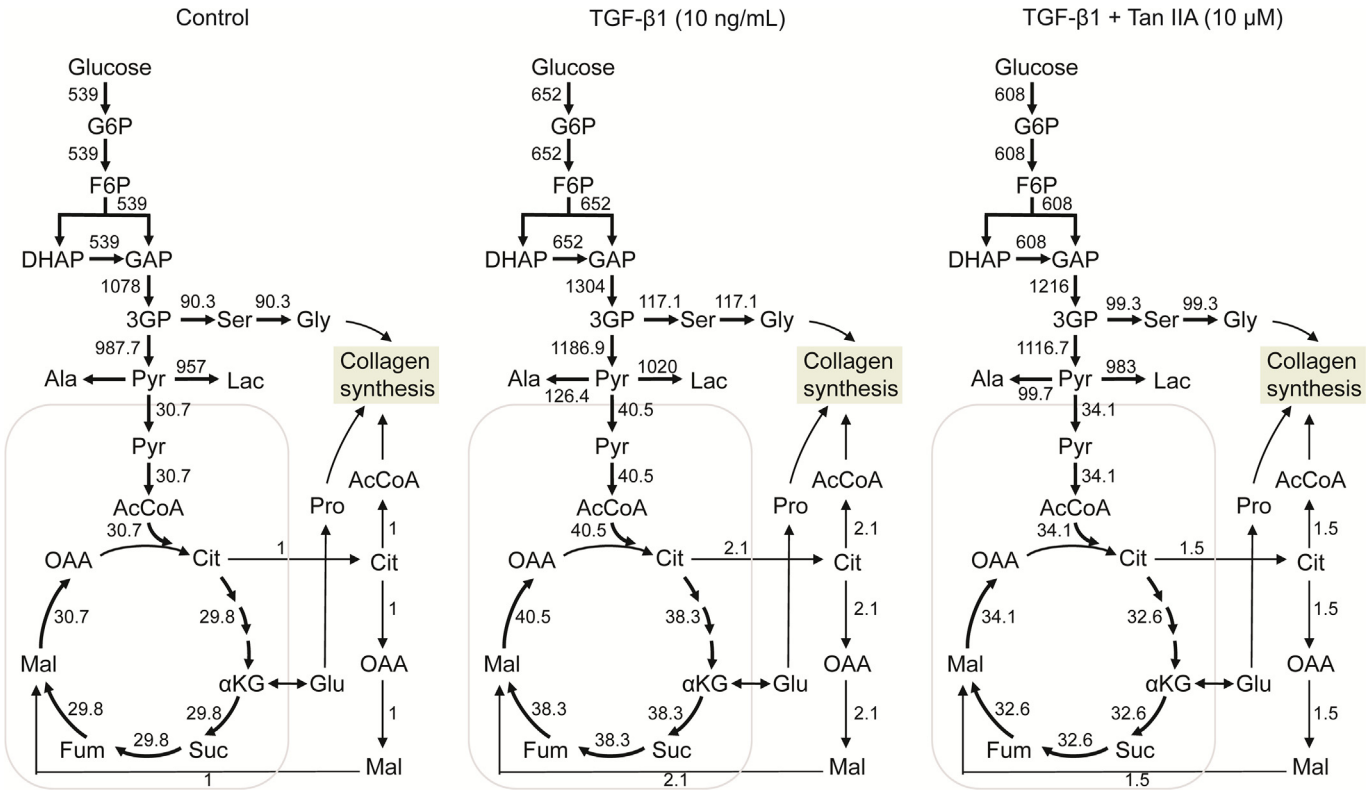

Fig. 4. Metabolic flux distributions in normal NIH-3T3 cells, NIH-3T3 cells induced by transforming growth factor-β1 (TGF-β1), and NIH-3T3 cells induced by TGF-β1 treat with tanshinone IIA (Tan IIA) (10 μM). Fluxes were determined by glucose uptake and lactate secretion rates and isotopic labeling data from [U-^{13}C] glucose tracer experiments by glucose metabolic flux analysis (MFA).

key energy metabolites extracted from [U-^{13}C] glucose-cultured NIH-3T3 cells by GC-MS and LC-MS are shown in Figs. S5–S8, respectively. Ensuring a stable state of cellular isotopes is a prerequisite for successful MFA experiments. The time to reach the isotopic steady state was determined based on the change in metabolite ^{13}C labeling ratios over time. We extracted M+2 (malate) and M+3 (pyruvate) isotopic metabolites from [U-^{13}C]-glucose-cultured NIH-3T3 cells in 12 and 24 h, and MIDs were calculated. After 24 h of cell culture, the ^{13}C-labeled ratios of glycolysis and TCA first-cycle metabolites were relatively stable, indicating that the cells reached and maintained an isotopic steady state in 24 h. We exemplified the isotope-labeled mass spectrometry data and the peak areas of the corresponding labeled metabolites for three cellular metabolites (pyruvate, malate, and glutamate), which were detected by GC-MS and LC-MS, respectively. GC-MS identified peaks corresponding to specific metabolites, and the contribution of these peaks ranged from *m/z* 174 Da (unlabeled isotopes) to 177 Da (labeled isotopes) (TBDMS-derivatized ^{13}C-labeled pyruvate), *m/z* 419–423 Da (TBDMS-derivatized ^{13}C-labeled malate), and *m/z* 432–437 Da (TBDMS-derivatized ^{13}C-labeled glutamate) based on known isotope masses (Fig. 2A). LC-MS identified specific metabolites, and the contribution of these peaks ranged from *m/z* 87 Da (unlabeled isotopes) to 90 Da (labeled isotopes) (^{13}C-labeled pyruvate), *m/z* 133–137 Da (^{13}C-labeled malate), and *m/z* 148–153 Da (^{13}C-labeled glutamate) based on known isotope masses (Fig. 2B). The areas under these peaks represented the measured ion counts for each isotope species, and their sum represented the total counts of the metabolites. The measured MIDs were finally converted into actual MID pairs for data interpretation by properly correcting for the natural isotopic contributions of different atoms in pyruvate, malate, and glutamate (Fig. 2C).

3.3. Disturbed glycolysis and TCA cycle flux of TGF-β1-induced PF

As shown in Fig. 3A, [U-^{13}C] glucose was used as a tracer to study the energy metabolism of TGF-β1-induced NIH-3T3 cells. The metabolites in glycolysis derived from [U-^{13}C] glucose were labeled as M+3 (pyruvate, lactate and alanine), whereas the metabolites in the first cycle of TCA derived from glucose were labeled as M+2 (α-ketoglutarate, fumarate, glutamate, malate, citrate, and aspartate). As shown in Fig. 3B, NIH-3T3 cells induced by TGF-β1 showed significant changes compared with the changes in the control cells after culture with [U-^{13}C] glucose. The levels of ^{13}C-labeled metabolites in glycolysis, *de novo* serine–glycine synthesis, and TCA cycle significantly increased, including M+3 isotopologs of pyruvate, lactate, alanine, and serine, and M+2 isotopologs of glycine, citrate, α-ketoglutarate, fumarate, malate, aspartate, proline, and glutamate. This indicated that the levels of carbon source from glucose entering the glycolysis and the TCA cycle increased after TGF-β1-induced PF. The total cellular concentration of ^{13}C-labeled and unlabeled metabolites represented the contribution of different carbon sources to the metabolites. As shown in Fig. 3C, the total cellular concentration of several metabolites in the glycolysis and TCA cycle significantly increased in model cells compared with control cells. The results were consistent with the increase in ^{13}C labeling rate (M+2 and M+3 isotopologs).

Next, we conducted ^{13}C-MFA to gain a deeper understanding of the metabolic effects of Tan IIA to further investigate the TGF-β1-induced fluxes of glycolysis and TCA metabolism in NIH-3T3 and

growth factor-β1 (TGF-β1) were treated with tanshinone IIA (Tan IIA) (5 μM and 10 μM) and incubated with [U-^{13}C] glucose for 24 h. Fraction of the labeled metabolites of M+2 and M+3 from [U-^{13}C] glucose in energy metabolism. (C) Total cellular relative level of metabolite in energy metabolism. $^{*}P < 0.05$, $^{**}P < 0.01$, $^{***}P < 0.001$, and $^{****}P < 0.0001$.

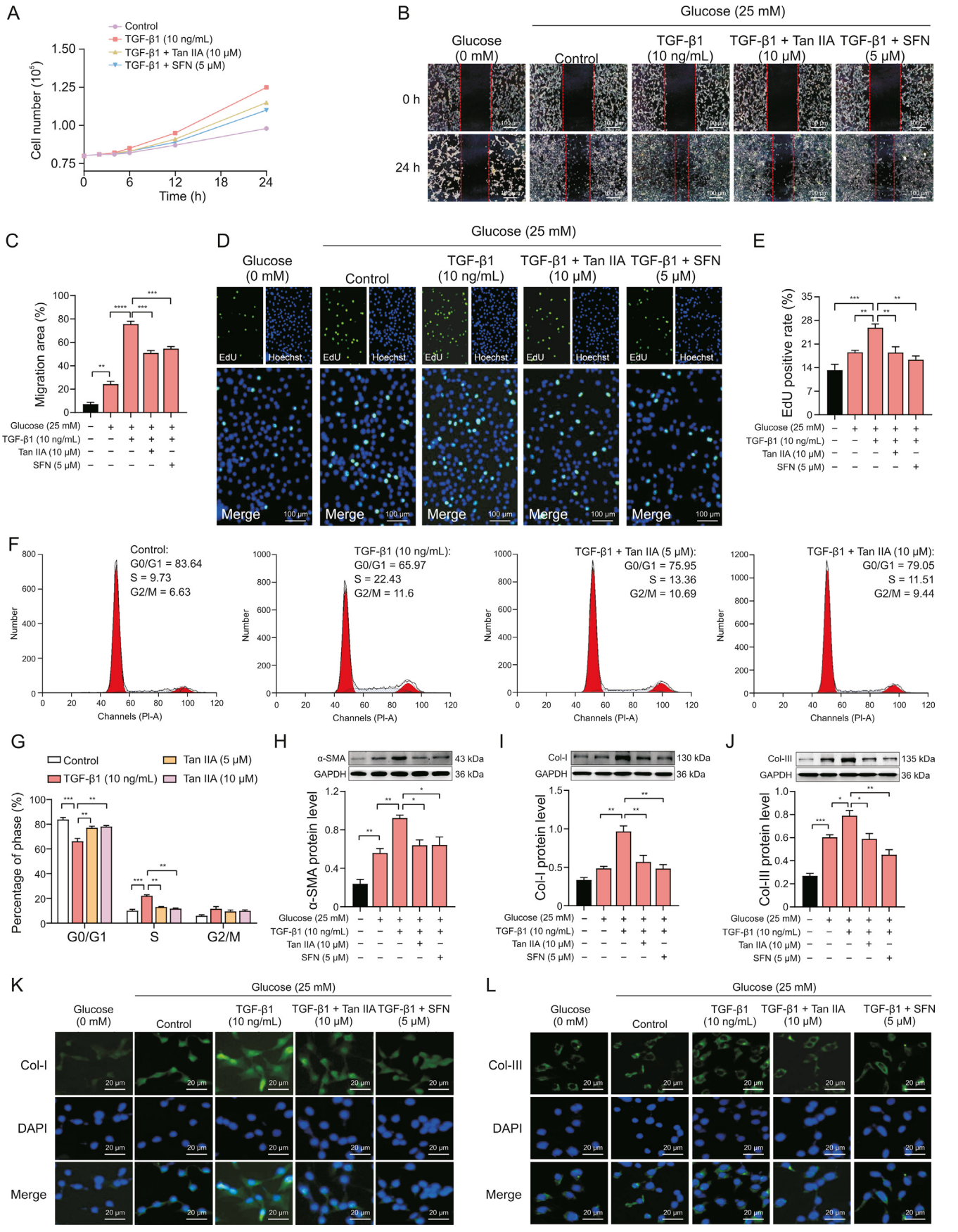

Fig. 5. Tanshinone IIA (Tan IIA) inhibits the proliferation and cell cycle of NIH-3T3 cells induced by transforming growth factor-β1 (TGF-β1) as well as reduces alpha-smooth muscle actin (α-SMA), collagen I (Col-I), and collagen III (Col-III) protein expression. (A) Number of NIH-3T3 cells induced by TGF-β1 treated with Tan IIA (10 μM) and sulforaphane (SFN)

to obtain quantitative maps of cellular metabolism in response to the assigned flux values in the network model. We first quantified the crosstalk between the cell and its environment (i.e., external rates, nutrient influx, and metabolic by-product secretion). The parameters required for calculating the rates of cell growth, nutrient influx, and secretion of metabolic by-products are depicted in Table S5. We calculated the glucose uptake and lactate secretion rates in NIH-3T3 cells, and the results are depicted in Fig. S9. Then, we created a ^{13}C-MFA model to enhance our analysis (Table S6). We corrected the natural isotope (Fig. S10) and optimized the model parameters during the analysis until a satisfactory fit to the data was achieved and the metabolic flux values could be estimated.

We next performed MFA to gain a better understanding of the metabolic consequences of TGF-β1 activation in fibroblasts. Steady-state metabolic fluxes were determined by fitting the measured extracellular rates and mass isotopomer distributions of intracellular metabolites and external lactate to a compartmentalized metabolic network model [27]. The combined labeling data from labeling experiments with [U-^{13}C] glucose tracers were integrated for this analysis, and statistically acceptable fits were obtained for all conditions. Overall, we observed that TGF-β1 stimulation increased intracellular metabolic fluxes, including *de novo* serine-glycine synthesis, glycolysis, TCA, and non-canonical TCA (Fig. 4).

3.4. Tan IIA attenuated TGF-β1-induced PF

Fibroblasts can proliferate and differentiate into numerous α-SMA-positive myofibroblasts when exposed to pathological factors such as TGF-β1. The aggressive phenotype of these myofibroblasts leads to the accumulation of type collagen, abnormal deposition of ECM, and acceleration of PF remodeling [28]. Previous studies found that Tan IIA could inhibit the growth of myofibroblasts in a dose-dependent manner [14]. This study found that Tan IIA and the positive drug SFN had a certain inhibitory effect on the growth of TGF-β1-induced myofibroblasts (Fig. 5A). NIH-3T3 cells were treated with Tan IIA for 24 h to investigate the anti-aggressive effect of Tan IIA in myofibroblasts. A two-dimensional scratch assay was performed. The results indicated that TGF-β1 could clearly improve the cell migration ability, and TGF-β1-induced cell migration was clearly inhibited when Tan IIA or SFN was added (Figs. 5B and C). The effect of Tan IIA on the DNA synthesis of myofibroblasts was detected by the EdU labeling experiment. We analyzed the cells using fluorescence microscopy after EdU labeling. The increase in the number of EdU-positive cells in fibroblasts induced by TGF-β1 indicated that TGF-β1 promoted cell proliferation (Figs. 5D and E). However, fewer fibroblasts in the Tan IIA or SFN group underwent cell division compared with those in the TGF-β1 group, indicating that the presence of Tan IIA or SFN inhibited cell proliferation. Next, we set out to explore the effects of Tan IIA on the cell cycle of myofibroblasts. NIH-3T3 cells were treated with Tan IIA for 24 h with indicated doses. Tan IIA induced cell cycle arrest in the G1 phase in NIH-3T3 cells (Figs. 5F and G). Additionally, we found that TGF-β1 increased the expression of α-SMA, Col-I and Col-III proteins in NIH-3T3 fibroblasts, and Tan IIA and SFN significantly inhibited the expression of α-SMA, Col-I, and Col-III proteins induced by TGF-β1 (Figs. 5H–J). We also found that Tan IIA could significantly reduce the increase in fluorescence intensity of collagen induced by TGF-β1 (Figs. 5K and L).

3.5. Tan IIA inhibited glycolysis and TCA cycle metabolic flux in NIH-3T3 cells

We used universally labeled [U-^{13}C] glucose as a tracer to track the cellular metabolism in glycolysis and TCA cycles after Tan IIA treatment to further study the effects of Tan IIA on the energy metabolism of myofibroblasts. We found that the amount of enriched labeled carbon in NIH-3T3 from the ^{13}C glucose increased on TGF-β1 stimulation (Fig. S11), indicating the presence of active glucose catabolism. Interestingly, we observed that the amount of enriched labeled carbon in glycolysis, *de novo* serine–glycine synthesis, and TCA cycle from ^{13}C glucose significantly reduced in a dose-dependent manner after treatment with Tan IIA, including pyruvate, lactate, and alanine from [U-^{13}C]-glucose; all decreased significantly in NIH-3T3 cells treated with Tan IIA, demonstrating that Tan IIA dose-dependently inhibited glycolysis. Pyruvate entered the TCA cycle through pyruvate dehydrogenase, generating M+2 metabolites (^{13}C labeled at two positions) in the first step. Similar results were observed for TCA cycles with M+2 labeled metabolites (malate, aspartate, fumarate, α-ketoglutarate, and glutamate) from [U-^{13}C] glucose after Tan IIA treatment. The results of Tan IIA treatment were evident in the decreased M+2 fraction of enriched labeled metabolites in the TCA cycle (Fig. 3B). Notably, we also analyzed the potential impact of Tan IIA on metabolic flux. We observed that the glucose uptake and lactate secretion rate of NIH-3T3 cells decreased by 6.7% and 3.6%, respectively, the *de novo* serine–glycine synthesis flux decreased by 15.2%, and the TCA flux decreased by 15.8% (Fig. 4). Therefore, the results indicated that Tan IIA might inhibit collagen production and cell activity by reducing the cellular metabolic flux of glycolysis and TCA.

3.6. Key enzymes in energy metabolism related to PF and Tan IIA activity

HK2 is a crucial enzyme in the initial stage of glycolysis. It catalyzes the conversion of glucose into glucose-6-phosphate and plays a significant role in the cellular uptake and utilization of glucose. Recent studies have reported increased transcripts encoding the major rate-regulating glycolytic enzyme HK2 in TGF-β1-stimulated PF [26]. We consistently observed that TGF-β1 significantly increased the expression of HK2, and Tan IIA inhibited the expression of HK2 in a dose-dependent manner (Fig. 6A). We next explored the upstream signaling pathway that affected the expression of HK2 to further understand the molecular mechanisms by which Tan IIA affected HK2. Previous studies showed that Tan IIA affected cell growth by inhibiting the PI3K/Akt/mTOR pathway [29]. Therefore, we examined the expression of PI3K/Akt/mTOR critical signaling proteins in Tan IIA-treated NIH-3T3 and MRC-5 cells. As shown in Figs. S12A–C, the expression of PI3K, *p*-Akt, and *p*-mTOR, as well as α-SMA, Col-I, and Col-III, in the Tan IIA and SFN treatment groups decreased in NIH-3T3 and MRC-5 cells, compared with the TGF-β1 group. Additionally, HIF-1α expression abnormally increased in various cancers, and HK2 was one of its downstream transcriptional targets [30]. Our study also revealed that Tan IIA reduced the protein expression of HIF-1α in NIH-3T3 and MRC-5 cells. Overall, these findings demonstrated that Tan IIA inhibited the PI3K/Akt/mTOR/HIF-1α pathway and down-regulated HK2 expression, decreasing of glycolysis and TCA metabolic flux and ultimately suppressing fibroblast growth.

(5 μM) within 24 h. (B, C) Tan IIA inhibited the migration of NIH-3T3 cells induced by TGF-β1. (D, E) Tan IIA reduced the percentage of 5-ethynyl-20-deoxyuridine (EdU) positive cells. (F, G) Cell cycle distribution of NIH-3T3 cells induced by TGF-β1 measured by flow cytometry after treatment with Tan IIA at doses of 5 and 10 μM. (H–J) Tan IIA decreased the expression of α-SMA, Col-I and Col-III protein by inhibiting the differentiation of fibroblasts into myofibroblasts. (K, L) Tan IIA reduced the fluorescence intensity of Col-I and Col-III protein. $^{*}P < 0.05$, $^{**}P < 0.01$, $^{***}P < 0.001$, $^{****}P < 0.0001$. DAPI: 4',6-diamidino-2-phenylindole.

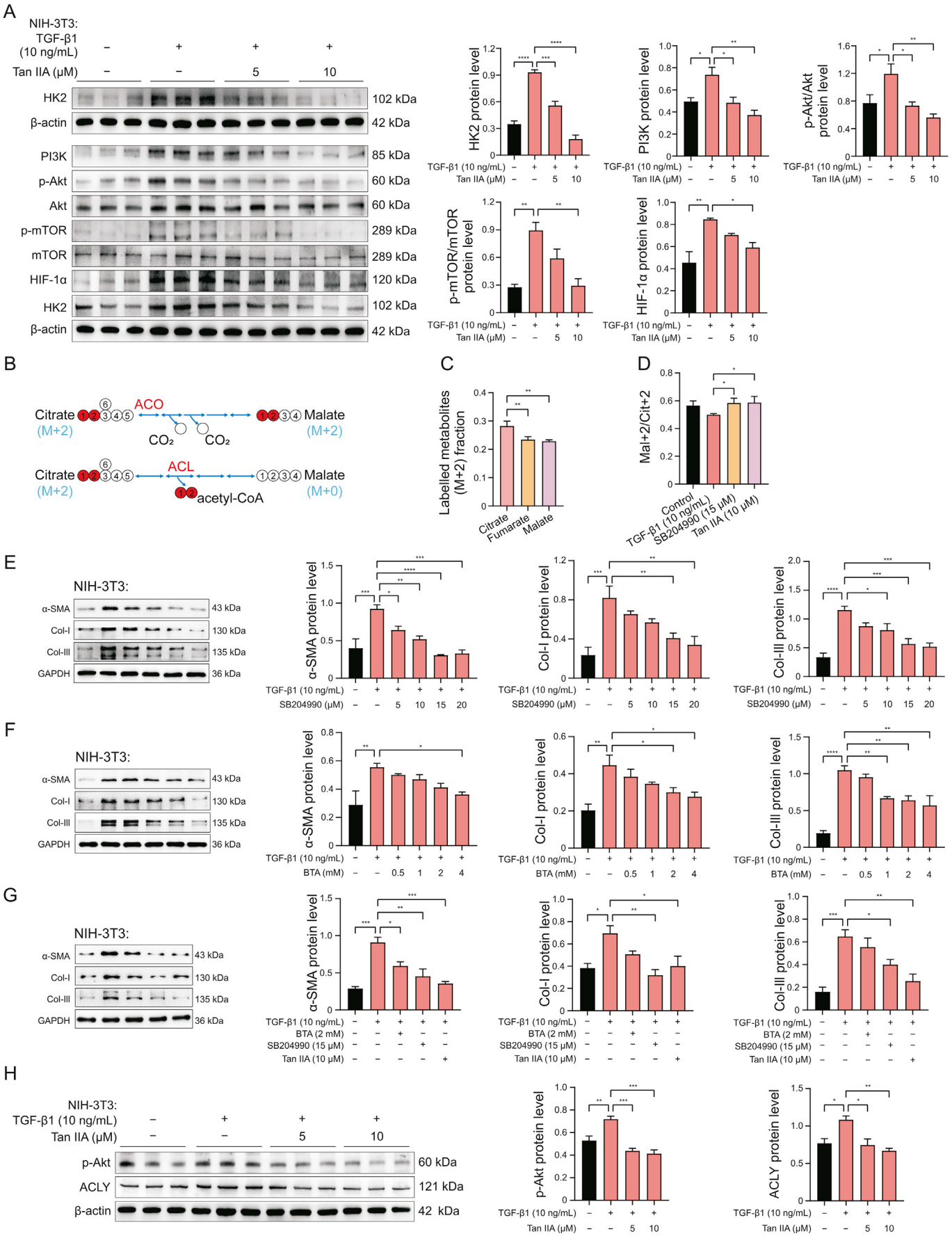
A
NIH-3T3:
TGF-β1 (10 ng/mL)
Tan IIA (μM)
HK2
β-actin
PI3K
p-Akt
Akt
p-mTOR
mTOR
HIF-1α
HK2
β-actin
102 kDa
42 kDa
85 kDa
60 kDa
60 kDa
289 kDa
289 kDa
120 kDa
102 kDa
42 kDa
HK2 protein level
PI3K protein level
p-Akt/Akt protein level
p-mTOR/mTOR protein level
HIF-1α protein level
B
Citrate (M+2)
ACO
CO2
Malate (M+2)
ACL
acetyl-CoA
Malate (M+0)
C
Labelled metabolites (M+2) fraction
Citrate
Fumarate
Malate
D
M+2/Cit+2
Control
TGF-β1 (10 ng/mL)
SB204990 (15 μM)
Tan IIA (10 μM)
E
NIH-3T3:
α-SMA
Col-I
Col-III
GAPDH
43 kDa
130 kDa
135 kDa
36 kDa
α-SMA protein level
Col-I protein level
Col-III protein level
SB204990 (μM)
F
BTA (mM)
G
BTA (2 mM)
SB204990 (15 μM)
Tan IIA (10 μM)
H
p-Akt
ACLY
β-actin
60 kDa
121 kDa
42 kDa
p-Akt protein level
ACLY protein level

3.7. Tan IIA regulated the non-canonical TCA cycle and inhibited collagen synthesis

When exported from mitochondria, citrate is broken down by ACLY to generate acetyl-CoA, which serves as a substrate for fatty acid synthesis. Evidence indicates that an imbalance of lipid mediators can drive fibrogenic responses [31]. However, the impact of this effect was reduced by the citrate carrier (CIC) (encoded by *Slc25a1*) inhibitor BTA and the ACLY inhibitor SB204990. The metabolism of the TCA cycle was monitored by following [U-^{13}C] glucose derived from the oxidative decarboxylation of pyruvate to produce citrate containing two heavy-labeled carbons (M+2 labeled citrate). Further metabolism by mitochondrial aconitase (ACO2) generated M+2-labeled TCA cycle intermediates, whereas the metabolism by ACL liberated M+2-labeled acetyl-CoA, thereby generating unlabeled oxaloacetate and downstream derivatives (Fig. 6B). Consequently, the reduction in M+2 labeling of TCA cycle intermediates downstream of citrate could potentially indicate the extent of cellular involvement in a non-canonical TCA cycle [32]. We found that the TGF-β1-stimulated NIH-3T3 cells exhibited a dissociation between M+2 citrate labeling and downstream metabolites (Fig. 6C). The mal+2/cit+2 ratio is useful in determining the extent to which malate is derived from the canonical TCA cycle [32]. Both the ACLY inhibitor (SB204990) and Tan IIA increased the mal+2/cit+2 ratio of NIH-3T3 (Fig. 6D). The concentrations of BTA and SB204990 used in the study were based on previous studies, and we also demonstrated their inhibitory effects on α-SMA release and collagen synthesis (Figs. 6E and F). Moreover, both BTA and SB204990 effectively suppressed the protein expression of α-SMA and collagen in NIH-3T3 and MRC-5 cells (Figs. 6G and Fig. S12D). Interestingly, we found that Tan IIA also dose-dependently inhibited ACLY expression, and Akt was one of its upstream transcriptional targets (Fig. 6H). This result was validated in both NIH-3T3 and MRC-5 cells (Figs. S12E and F). These findings suggested that Tan IIA might inhibit collagen synthesis in myofibroblasts by blocking cytosol citrate decomposition.

3.8. Tan IIA inhibited PI3K/Akt/mTOR/HIF-1α/HK2 pathway activities, as well as glycolysis and collagen synthesis in BLM-induced mouse model

Next, we employed BLM-induced PF mouse model to further investigate whether Tan IIA exerted its anti-PF effect by inhibiting PI3K/Akt/mTOR/HIF-1α/HK2 pathway activities *in vivo*. After an intratracheal spray of BLM, vehicle, 10 and 20 mg/kg of Tan IIA were administered daily through gavage (Fig. 7A). H&E staining results revealed that the lung structure of mice in the BLM-treated group was severely damaged, and the alveolar walls were evidently thickened. However, fibrosis showed apparent symptomatic relief in the Tan IIA treatment group compared with the BLM group (Fig. 7B). Furthermore, the expression of Col-I, Col-III, and α-SMA proteins also increased in the BLM group compared with the control group. 20 mg/kg Tan IIA alleviated collagen deposition significantly (Fig. 7C). Interestingly, PI3K, *p*-Akt, *p*-mTOR, HIF-1α and HK2 expression levels also decreased in the lung tissues of BLM-induced PF mice following treatment with Tan IIA (Fig. 7D). Therefore, we speculated that the inhibition of the PI3K/Akt/mTOR/HIF-1α/HK2 pathway might prevent the enhancement of glycolysis in mice with BLM-induced PF. Consistent with the results *in vitro*, we also found increased ACLY expression in lung tissues of mice with BLM-induced PF, which was alleviated by Tan IIA administration (Fig. 7E).

4. Discussion

PF is a progressive and intractable lung disease characterized by exaggerated inflammatory and fibrotic responses, leading to pulmonary fibrotic remodeling and ECM deposition [33]. Despite considerable improvements in PF treatment, the 5-year survival rate is still unsatisfactory due to limited clinical drug treatment. Tan IIA, the most important active component extracted from *Salvia miltiorrhiza*, has been found to display potent anti-fibrotic effects primarily due to its antioxidant and anti-inflammatory properties [34]. Recent studies have demonstrated that metabolic reprogramming or dysregulation is one of the risk factors of PF, which plays a profibrotic role by affecting pathological mechanisms [4], and targeting metabolic reprogramming has been explored as a potential therapeutic strategy against PF. This study was novel in characterizing the effects of Tan IIA on ^{13}C metabolic flux in TGF-β1 induced NIH-3T3. We found that Tan IIA significantly inhibited myofibroblast growth, glycolysis, and TCA metabolism by inhibiting the activity of key rate-regulating glycolytic enzyme HK2. Notably, we demonstrated that Tan IIA reduced collagen synthesis caused by cytoplasmic citrate consumption and acetyl coenzyme production by inhibiting ACLY. These anti-PF effects were demonstrated in the BLM-induced PF mouse model.

Metabolic reprogramming inhibition has been explored as an appealing therapeutic strategy in PF based on the understanding of the pro-survival role of metabolic reprogramming in PF under various stresses. Metabolic reprogramming is a fundamental characteristic of cancer, which involves an increase in glucose uptake and a preference for utilizing glucose through aerobic glycolysis [35]. Increasing evidence suggests that metabolic reprogramming may also play a significant role in developing fibrosis besides cancer [36]. The study also found that the change in glycolysis might be a remarkable feature of various fibrosis diseases [37]. Glucose uptake is the first rate-limiting step in glycolysis. *In vitro* studies in human PF showed that TGF-β1 stimulated glucose uptake at both the protein and mRNA levels [4]. Further, the TCA cycle is essential for cellular oxidative phosphorylation, and its up-regulation facilitates cellular redox balance and energy production. The evidence suggests that both myofibroblasts and TGF-β1-induced human PF exhibit a glycolytic phenotype and also increase mitochondrial respiration, leading to ATP and TCA carbon intermediate production. These findings support the notion that these cells are involved in multiple fibrotic responses [10,38]. However, most studies often involve general cell metabolism measurement to determine glycolysis flux, mitochondrial respiration, and glycolysis inhibition by genetic and pharmacological methods to prove the key role of glycolysis in PF. Beyond the mere network structure, we need to understand how the components work together to produce appropriate network responses that enable cellular functioning under ever-changing environmental conditions [39].

Similar to cancer cells, the metabolism of myofibroblasts is significantly different from that of normal cells, enabling fibrotic cells to adapt to changing microenvironments and maintain rapid

Fig. 6. Tanshinone IIA (Tan IIA) inhibits the expression of key enzymes and reduces collagen synthesis. (A) Tan IIA inhibits the expression of hexokinase 2 (HK2) by regulating phosphoinositide 3-kinase (PI3K)/protein kinase B (Akt)/mammalian target of rapamycin (mTOR)/hypoxia-inducible factor 1α (HIF-1α) pathway. (B) Schematic representation of the possible fate of 2-carbon citrate derived from [U-^{13}C] glucose. (C) Fractional m+2 enrichment of tricarboxylic acid (TCA)-cycle intermediates in NIH-3T3 cells induced by transforming growth factor-β1 (TGF-β1) cultured with [U-^{13}C] glucose for 24 h. (D) Fractional enrichment of glucose-derived malate M+2 relative to citrate M+2 (mal+2/cit+2) in NIH-3T3 cells induced by TGF-β1 after incubation with Tan IIA (10 μM) or SB204990 (15 μM) for 24 h. (E) ATP-citrate lyase inhibitors dose-dependently inhibit α-smooth muscle actin (α-SMA) and collagen synthesis. (F) SLC25A1 inhibition reduced citrate cytoplasmic transport, and reduced α-SMA and collagen synthesis. (G) Blocking mitochondrial citric acid efflux and decomposition can reduce α-SMA and collagen synthesis. BTA (2 mM) and SB204990 (15 μM) can effectively inhibit α-SMA and collagen synthesis. (H) Tan IIA inhibited the expression of *p*-Akt and ACLY in a concentration dependent manner. $^{*}P < 0.05$, $^{**}P < 0.01$, $^{***}P < 0.001$, $^{****}P < 0.0001$.

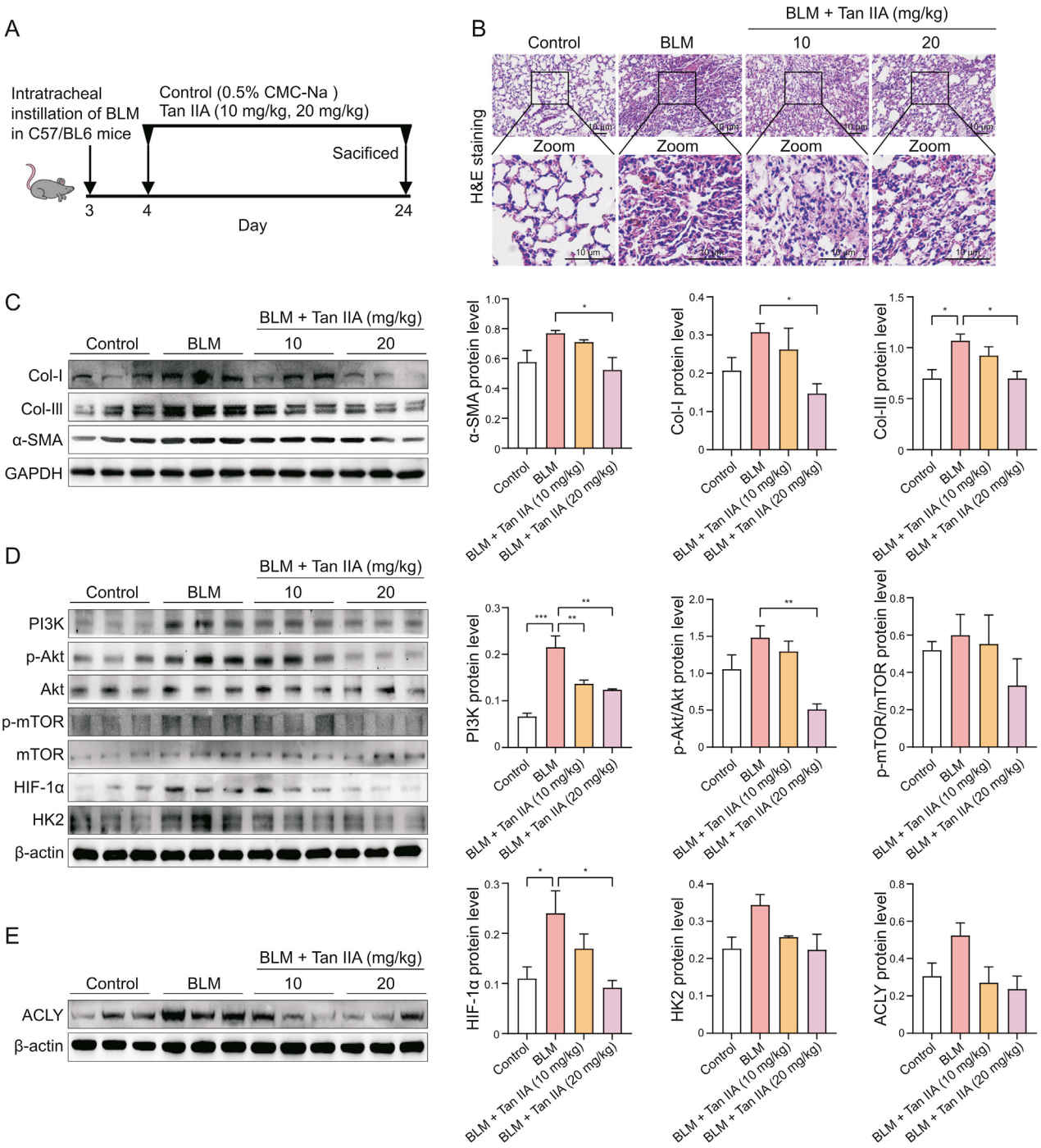

Fig. 7. Tanshinone IIA (Tan IIA) alleviates pulmonary fibrosis (PF) in bleomycin (BLM)-induced mouse model. (A) Schematic workflow for BLM-induced PF mouse model. After intratracheal instillation of BLM, C57BL/6 mice were given 0.5% CMC-Na, Tan IIA (10 mg/kg, 20 mg/kg) by gavage the next day for 21 days. (B) Histopathological changes of lung tissue of mice in different groups. (C) Western blot analysis of the expression levels of alpha-smooth muscle actin (α-SMA), collagen I (Col-I), and collagen III (Col-III) in mouse lungs of different groups. Quantitative results are presented as mean ± standard deviation (SD) of the index's relative protein levels. (D) Western blot analysis of the proteins expression levels of phosphoinositide 3-kinase (PI3K)/protein kinase B (Akt)/mammalian target of rapamycin (mTOR)/hypoxia-inducible factor 1α (HIF-1α)/hexokinase 2 (HK2) pathway in mouse lungs of different groups. (E) Western blot analysis of the proteins expression levels of ACLY in mouse lungs of different groups. $^{*}P < 0.05$, $^{**}P < 0.01$, $^{***}P < 0.001$. GAPDH: glyceraldehyde 3-phosphate dehydrogenase.

proliferation. In the last decade, stable isotope tracing and network analysis became effective tools for revealing metabolic pathways that are differentially activated in cancer cells. Especially, ^{13}C-MFA has became a significant technique for quantifying intracellular fluxes in cancer cells [18]. With the aid of 100% ^{13}C glucose tracers and network analysis, combined with the measurement of lactate labeling, the metabolic pathways activated in fibroblasts and the effect of Tan IIA on these metabolic pathways were determined for the first time. Further, the absolute fluxes of glycolysis, serine and glycine metabolism, and TCA pathway were accurately calculated using the user-friendly ^{13}C-MFA software tool isotopomer network compartmental analysis (INCA). In this study, using a [U-^{13}C]-glucose

isotope tracing MFA technique, we found that the energy metabolic flux of TGF-β1-induced PF significantly increased. Glucose, as a source of carbon in glycolysis, was promoted. A large amount of pyruvate was produced downstream, and the proportions of the intermediates entering the downstream TCA cycle significantly increased. Myofibroblast enhanced anaplerosis from carbon sources to maintain an energy supply, resulting in a continuous rise in the total cellular concentration of downstream metabolite. However, the exposure of Tan IIA decreased the glycolysis and TCA cycle flux compared with that in the model cells, indicating the inhibition of effective metabolic reprogramming by Tan IIA treatment.

We further clarified the underlying mechanism and downstream signaling events leading to the inhibition of metabolic reprogramming by Tan IIA. The promotion of glycolysis is typically achieved by increasing the production of glycolytic enzymes. One such enzyme, HK2, plays a crucial role in glucose metabolism by catalyzing the first step through the phosphorylation of glucose. The abundance of transcripts encoding the key rate-regulating glycolytic enzyme HK2 increased in TGF-β1-stimulated PF [7,26,40]. Furthermore, TGF-β1 activated Akt by inducing phosphorylation of the serine/threonine kinase Akt in fibroblasts [41]. Akt is crucial in regulating several cellular processes such as cell survival, proliferation, and metabolism. Targeting the overactive Akt pathway as a potential treatment for PF has been investigated with some success [42,43]. Akt can regulate HK2 expression and activity by upregulating of HIF-1α through mTORC1 activation, promoting cell viability and DNA synthesis [44]. Recent research has highlighted the importance of metabolic perturbations in developing this condition, including the significantly increased levels of phosphorylated Akt in both PF and activated myofibroblasts [43,45,46]. Based on this understanding, it is possible that reducing Akt phosphorylation or blocking glycolytic flux can be a promising new strategy for Tan IIA to slow the progression of PF. Traditional Chinese medicine (TCM) and its bioactive ingredients usually affect multiple metabolic targets to exert effects. For example, studies found that multiple components, including matrine, oleanolic acid, dioscin, and chrysin, could suppress tumor proliferation by inhibiting HIF-1α and HK2 expression [47]. Similarly, we found that Tan IIA could inhibit the expression of PI3K/Akt/mTOR/HIF-1α/HK2 pathway in fibroblasts in a dose-dependent manner, thereby reducing glycolysis and TCA. The results of these cell experiments were further confirmed in mice.

The mitochondrial CIC diverts metabolic flux away from mitochondria, suggesting a potential breakpoint in the TCA cycle. The CIC exports citrate from mitochondria, and the acetyl-CoA generated in the cytosol is further processed and incorporated into the biosynthesis of fatty acids [20]. ACLY, regulated by Akt, is an enzyme upstream of acetyl-CoA carboxylase that converts citrate derived from the TCA cycle into cytosolic acetyl-CoA and oxaloacetate [48]. These provide the necessary cytoplasmic acetyl-CoA for protein acetylation and lipid biosynthesis [49]. The fact that ACLY is interdependent on TCA cycle enzymes indicates that it can also meet cellular metabolic demands by creating an atypical TCA cycle that enables continuous oxaloacetate regeneration for citrate production [32]. Importantly, the genetic interference of ACL or treatment with ACLi suppressed TGF-β1-induced cell proliferation, myofibroblast formation, and ECM production in NIH-3T3 fibroblasts [48]. Consistently, we found that both the CIC inhibitor BTA and the ACLY inhibitor SB204990 reduced TGF-β1-induced α-SMA and collagen expression. Notably, we found that Tan IIA could inhibit the expression of ACLY in a dose-dependent manner. This study was novel in revealing that Tan IIA had regulatory ACLY activity in fibrillogenesis. These data indicated that inhibiting ACLY might be an effective approach for treating PF.

5. Conclusion

We have revealed a novel mechanism for the anti-PF of Tan IIA, beyond its proven anti-inflammatory and antioxidant effects, by combining ^{13}C-MFA and pharmacological methods. This study indicated that Tan IIA reduced metabolic fluxes in the glycolysis and TCA cycle by inhibiting the hyperactive PI3K/Akt/mTOR/HIF-1α/HK2 pathway. We further found that Tan IIA inhibited cytoplasmic citrate catabolism by downregulating ACLY expression *in vivo* and *in vitro*, and metabolically inhibited the biosynthesis of fatty acids required for collagen synthesis. This study was novel in exploring the mechanism of the occurrence and development of Tan IIA in treating of PF using ^{13}C-MFA technology, which provided not only direct evidence for the participation of Tan IIA in modulating energy metabolism in treating PF but also details on the mechanism of action of TCM based on ^{13}C-MFA.

CRediT author statement

Baixi Shan: Methodology, Investigation, Data curation visualization, and Writing - original draft preparation; **Haoyan Zhou:** Methodology, Investigation, and Data curation; **Congying Guo:** Investigation and Methodology; **Xiaolu Liu:** Investigation; **Mingyu Wu:** Investigation; **Rao Zhai:** Investigation; **Jun Chen:** Resources, Supervision, and Funding acquisition.

Declaration of competing interest

The authors declare that there are no conflicts of interest.

Acknowledgments

This work was financially supported by the National Natural Science Foundation of China (Grant No.: 82174100). The authors thank Nian Wang and Zi-Yuan Wang for technical support from the Center for Analysis and Testing of China Pharmaceutical University.

Appendix A. Supplementary data

Supplementary data to this article can be found online at https://doi.org/10.1016/j.jpha.2023.09.008.

References

[1] R. Rajesh, R. Atallah, T. Bärnthaler, Dysregulation of metabolic pathways in pulmonary fibrosis, Pharmacol. Ther. 246 (2023), 108436.
[2] H. Zhao, P.A. Dennery, H. Yao, Metabolic reprogramming in the pathogenesis of chronic lung diseases, including BPD, COPD, and pulmonary fibrosis, Am. J. Physiol. Lung Cell. Mol. Physiol. 314 (2018) L544–L554.
[3] T. Kinoshita, T. Goto, Molecular mechanisms of pulmonary fibrogenesis and its progression to lung cancer: A review, Int. J. Mol. Sci. 20 (2019), 1461.
[4] B. Selvarajah, I. Azuelos, D. Anastasiou, et al., Fibrometabolism-An emerging therapeutic frontier in pulmonary fibrosis, Sci. Signal. 14 (2021), eaay1027.
[5] S. Saito, A. Alkhatib, J.K. Kolls, et al., Pharmacotherapy and adjunctive treatment for idiopathic pulmonary fibrosis (IPF), J. Thorac. Dis. 11 (2019) S1740–S1754.
[6] L.A.J. O'Neill, R.J. Kishton, J. Rathmell, A guide to immunometabolism for immunologists, Nat. Rev. Immunol. 16 (2016) 553–565.
[7] B. Selvarajah, I. Azuelos, M. Platé, et al., mTORC1 amplifies the ATF4-dependent *de novo* serine-glycine pathway to supply glycine during TGF-β_1-induced collagen biosynthesis, Sci. Signal. 12 (2019), eaav3048.
[8] R.C. Chambers, P.F. Mercer, Mechanisms of alveolar epithelial injury, repair, and fibrosis, Ann. Am. Thorac. Soc. 12 (2015) S16–S20.
[9] C. Vancheri, Common pathways in idiopathic pulmonary fibrosis and cancer, Eur. Respir. Rev. 22 (2013) 265–272.
[10] N. Xie, Z. Tan, S. Banerjee, et al., Glycolytic reprogramming in myofibroblast differentiation and lung fibrosis, Am. J. Respir. Crit. Care Med. 192 (2015) 1462–1474.
[11] M. Andrianifahanana, D.M. Hernandez, X. Yin, et al., Profibrotic up-regulation of glucose transporter 1 by TGF-β involves activation of MEK and mammalian target of rapamycin complex 2 pathways, Faseb. J. 30

(2016) 3733–3744.
[12] H. He, H. Tang, L. Gao, et al., Tanshinone IIA attenuates bleomycin-induced pulmonary fibrosis in rats, Mol. Med. Rep. 11 (2015) 4190–4196.
[13] F. Feng, N. Li, P. Cheng, et al., Tanshinone IIA attenuates silica-induced pulmonary fibrosis via inhibition of TGF-β1-Smad signaling pathway, Biomed. Pharmacother. 121 (2020), 109586.
[14] L. An, L.Y. Peng, N.Y. Sun, et al., Tanshinone IIA activates nuclear factor-erythroid 2-related factor 2 to restrain pulmonary fibrosis via regulation of redox homeostasis and glutaminolysis, Antioxid. Redox Signal. 30 (2019) 1831–1848.
[15] Z. Wang, F. Zhang, W. Liu, et al., Impaired tricarboxylic acid cycle flux and mitochondrial aerobic respiration during isoproterenol induced myocardial ischemia is rescued by bilobalide, J. Pharm. Anal. 11 (2021) 764–775.
[16] M. Yuan, D.M. Kremer, H. Huang, et al., *Ex vivo* and *in vivo* stable isotope labelling of central carbon metabolism and related pathways with analysis by LC-MS/MS, Nat. Protoc. 14 (2019) 313–330.
[17] Y. Toya, N. Kono, K. Arakawa, et al., Metabolic flux analysis and visualization, J. Proteome Res. 10 (2011) 3313–3323.
[18] M.R. Antoniewicz, A guide to ^{13}C metabolic flux analysis for the cancer biologist, Exp. Mol. Med. 50 (2018) 1–13.
[19] C.P. Long, M.R. Antoniewicz, High-resolution ^{13}C metabolic flux analysis, Nat. Protoc. 14 (2019) 2856–2877.
[20] Y. Li, Y.C. Li, X.T. Liu, et al., Blockage of citrate export prevents TCA cycle fragmentation *via* Irg1 inactivation, Cell Rep. 38 (2022), 110391.
[21] Y. Zhang, G. Yu, H. Chu, et al., Macrophage-associated PGK1 phosphorylation promotes aerobic glycolysis and tumorigenesis, Mol. Cell 71 (2018) 201–215.
[22] G.F. Zhang, M.V. Jensen, S.M. Gray, et al., Reductive TCA cycle metabolism fuels glutamine- and glucose-stimulated insulin secretion, Cell Metab. 33 (2021) 804–817.
[23] B. Shan, M. Wu, T. Chen, et al., Berberine attenuates hyperuricemia by regulating urate transporters and gut microbiota, Am. J. Chin. Med. 50 (2022) 2199–2221.
[24] B. Shan, Z. Ai, S. Zeng, et al., Gut microbiome-derived lactate promotes to anxiety-like behaviors through GPR81 receptor-mediated lipid metabolism pathway, Psychoneuroendocrinology 117 (2020), 104699.
[25] H. Li, M. Wu, C. Guo, et al., Tanshinone IIA regulates Keap1/Nrf2 signal pathway by activating Sestrin2 to restrain pulmonary fibrosis, Am. J. Chin. Med. 50 (2022) 2125–2151.
[26] R. Nigdelioglu, R.B. Hamanaka, A.Y. Meliton, et al., Transforming growth factor (TGF)-β promotes *de novo* serine synthesis for collagen production, J. Biol. Chem. 291 (2016) 27239–27251.
[27] D. DeWaal, V. Nogueira, A.R. Terry, et al., Hexokinase-2 depletion inhibits glycolysis and induces oxidative phosphorylation in hepatocellular carcinoma and sensitizes to metformin, Nat. Commun. 9 (2018), 446.
[28] H. Liu, X. Zhang, Y. Shao, et al., Danshensu alleviates bleomycin-induced pulmonary fibrosis by inhibiting lung fibroblast-to-myofibroblast transition via the MEK/ERK signaling pathway, Bioengineered 12 (2021) 3113–3124.
[29] H. Liu, C. Liu, M. Wang, et al., Tanshinone IIA affects the malignant growth of Cholangiocarcinoma cells by inhibiting the PI3K-Akt-mTOR pathway, Sci. Rep. 11 (2021), 19268.
[30] T. Zhang, X. Zhu, H. Wu, et al., Targeting the ROS/PI3K/AKT/HIF-1α/HK2 axis of breast cancer cells: Combined administration of Polydatin and 2-Deoxy-d-glucose, J. Cell Mol. Med. 23 (2019) 3711–3723.
[31] A. Mamazhakypov, R.T. Schermuly, L. Schaefer, et al., Lipids - two sides of the same coin in lung fibrosis, Cell. Signal. 60 (2019) 65–80.
[32] P.K. Arnold, B.T. Jackson, K.I. Paras, et al., A non-canonical tricarboxylic acid cycle underlies cellular identity, Nature 603 (2022) 477–481.
[33] J. Li, X. Zhai, X. Sun, et al., Metabolic reprogramming of pulmonary fibrosis, Front. Pharmacol. 13 (2022), 1031890.
[34] F. Feng, P. Cheng, S. Xu, et al., Tanshinone IIA attenuates silica-induced pulmonary fibrosis via Nrf2-mediated inhibition of EMT and TGF-β1/Smad signaling, Chem. Biol. Interact. 319 (2020), 109024.
[35] N. Wang, H. Liu, G. Liu, et al., Yeast β-D-glucan exerts antitumour activity in liver cancer through impairing autophagy and lysosomal function, promoting reactive oxygen species production and apoptosis, Redox Biol. 32 (2020), 101495.
[36] Z. Chen, M. Liu, L. Li, et al., Involvement of the Warburg effect in non-tumor diseases processes, J. Cell. Physiol. 233 (2018) 2839–2849.
[37] X. Zhao, P. Psarianos, L.S. Ghoraie, et al., Metabolic regulation of dermal fibroblasts contributes to skin extracellular matrix homeostasis and fibrosis, Nat. Metab. 1 (2019) 147–157.
[38] K. Bernard, N.J. Logsdon, S. Ravi, et al., Metabolic reprogramming is required for myofibroblast contractility and differentiation, J. Biol. Chem. 290 (2015) 25427–25438.
[39] N. Zamboni, S.M. Fendt, M. Rühl, et al., ^{13}C-based metabolic flux analysis, Nat. Protoc. 4 (2009) 878–892.
[40] X. Yin, M. Choudhury, J.H. Kang, et al., Hexokinase 2 couples glycolysis with the profibrotic actions of TGF-β, Sci. Signal. 12 (2019), eaax4067.
[41] W. Qian, X. Cai, Q. Qian, et al., Astragaloside IV modulates TGF-β1-dependent epithelial-mesenchymal transition in bleomycin-induced pulmonary fibrosis, J. Cell. Mol. Med. 22 (2018) 4354–4365.
[42] J. Wang, K. Hu, X. Cai, et al., Targeting PI3K/AKT signaling for treatment of idiopathic pulmonary fibrosis, Acta Pharm. Sin. B 12 (2022) 18–32.
[43] X. Hu, Q. Xu, H. Wan, et al., PI3K-Akt-mTOR/PFKFB$_3$ pathway mediated lung fibroblast aerobic glycolysis and collagen synthesis in lipopolysaccharide-induced pulmonary fibrosis, Lab. Invest. 100 (2020) 801–811.
[44] Q. Lou, M. Zhang, K. Zhang, et al., Arsenic exposure elevated ROS promotes energy metabolic reprogramming with enhanced AKT-dependent HK2 expression, Sci. Total Environ. 836 (2022), 155691.
[45] Y. Ji, Y.N. Dou, Q.W. Zhao, et al., Paeoniflorin suppresses TGF-β mediated epithelial-mesenchymal transition in pulmonary fibrosis through a Smad-dependent pathway, Acta Pharmacol. Sin. 37 (2016) 794–804.
[46] H.S. Hsu, C.C. Liu, J.H. Lin, et al., Involvement of ER stress, PI3K/AKT activation, and lung fibroblast proliferation in bleomycin-induced pulmonary fibrosis, Sci. Rep. 7 (2017), 14272.
[47] S. Wang, J.L. Fu, H.F. Hao, et al., Metabolic reprogramming by traditional Chinese medicine and its role in effective cancer therapy, Pharmacol. Res. 170 (2021), 105728.
[48] M. Imamura, J.S. Moon, K.P. Chung, et al., RIPK$_3$ promotes kidney fibrosis via AKT-dependent ATP citrate lyase, JCI Insight 3 (2018), e94979.
[49] G. Hatzivassiliou, F. Zhao, D.E. Bauer, et al., ATP citrate lyase inhibition can suppress tumor cell growth, Cancer Cell 8 (2005) 311–321.